Journal of Applied Physics ARTICLE pubs.aip.org/aip/jap

Transport of *p–n* junction in complex honeycomb lattice

Cite as: J. Appl. Phys. **138**, 184302 (2025); doi: 10.1063/5.0303917
Submitted: 25 September 2025 · Accepted: 22 October 2025 ·
Published Online: 10 November 2025

Yao Zhang, Xing Wang, and Yu-Xian Li[a)]

AFFILIATIONS

College of Physics and Hebei Advanced Thin Films Laboratory, Hebei Normal University, Shijiazhuang, Hebei 050024, China

[a)]**Author to whom correspondence should be addressed:** yxli@mail.hebtu.edu.cn

ABSTRACT

We investigate electron transport through the *p–n* junction of a complex honeycomb (CHC) lattice under a vertical magnetic field, where *m* atoms are added to each side of the hexagonal honeycomb lattice (with $m = 0$ corresponding to graphene). Using the tight-binding model and Landauer–Büttiker formalism, and non-equilibrium Green's function method, we study the conductance of clean and disordered CHC lattices. For clean CHC lattices, equidistant plateaus appear in the *n–n* junctions. The conductance plateau values of $m = 0$ and $m = 2$ lattices are $(2n + 1) \cdot 2e^2/h$, while those for $m = 1$ and $m = 3$ lattices are $n \cdot 2e^2/h$ (n = 0, 1, 2, ...). In the *p–n* region, the partial conductance of the CHC lattice is caused by Klein tunneling, and the lattice conductance of $m = 1$ and $m = 3$ exhibits oscillations. For the disordered $m = 1$ CHC lattice, a bidirectional conduction channel is formed near right lead energy $E_R = 0$. For CHC lattices with a magnetic field, disorder can enhance conductance, but the ideal plateau only exists within a certain range of disorder intensity.

I. INTRODUCTION

The lattice structure of graphene has long been a focus of research.[1–9] The unique energy band structure of graphene gives rise to distinctive properties near the Dirac point. Owing to its linear dispersion relation, electrons in graphene behave as massless relativistic particles at low energies, described by the Dirac equation.[10,11] The quantum Hall plateau exhibits that the semi-integer value is $g(n + 1/2)e^2/h$, where the degeneracy is $g = 4$. By tuning the gate voltage, the carrier type of graphene can be switched between electron and hole conduction. This unique bipolar characteristic makes the graphene *p–n* junction an ideal platform for studying the electron–hole quasiparticle interaction.[12–14] Graphene *p–n* junction[15] has been successfully fabricated, and its conductance at both ends exhibits unique quantized conductance behavior under the quantum Hall regime: for *p–p* or *n–n* junctions, the conductance plateau values are semi-integer, given by $4(n + 1/2)e^2/h$.[16] For disordered *p–n* junctions, new conductance plateaus appear at e^2/h and $(3/2)e^2/h$. The emergence of these plateaus arises from the mixing of edge states of electrons and holes at the interface.[17] Graphene research also reveals special quantum phenomena, such as the anomalous quantum Hall effect[18,19] and the Klein tunneling effect.[20]

Recently, graphene-like lattices have also attracted widespread attention. The Dice lattice,[21] for example, is a typical graphene-like honeycomb lattice, with an extra central atom at the center of each original hexagon. In the Brillouin zone, a flatband exists at the K and K' points that passes through two Dirac bands. The low-energy excitations of the Dice lattice are described by the Dirac-well equation, with pseudospin $S = 1$.[22–24] Lee *et al.*[25] and others proposed a new material model that enables multiple robust flatbands in a single system, and these flatbands are shown to be unaffected by strong interactions. This material system takes the near-commensurate charge density wave phase of 1T-TaS_2 as a prototype,[26–28] and its structure can be regarded as a honeycomb superlattice (HCS) similar to graphene lattice. Specifically, *m* additional atoms are introduced on each edge of the conventional hexagonal honeycomb lattice.[29,30] This kind of honeycomb lattice exhibits distinctive electronic structure properties: when *m* is odd, a flatband emerges at the band center ($E = 0$). Unlike traditional graphene, only a single valley-polarized Dirac cone appears. For $m > 1$, additional band modulation is introduced.[31,32] The special structure of this honeycomb lattice provides an ideal platform for investigating new Dirac electron transport phenomena.

In this work, we study electron transport through the complex honeycomb (CHC) lattice p–n junction under a perpendicular magnetic field B. By using the tight-binding model and the non-equilibrium Green's function method,[33–35] the conductance is calculated. We find that equidistant plateaus appear in n–n junctions, and the conductance values of CHC lattices with $m = 1, 2, 3$ are higher than those with $m = 0$. In p–n junction, part of the conductance of the CHC lattices arises from the Klein tunneling effect. When a perpendicular magnetic field is applied, the conductance is also influenced by mixed electron–hole Hall edge states. New conductance plateaus emerge with the introduction of disorder.

The rest of the paper is organized as follows. In Sec. II, we introduce the Hamiltonian and energy bands of the CHC lattice, along with the formulas and methods employed to calculate the conductance of the p–n junction. The numerical results are discussed in Sec. III. Finally, a brief summary is provided in Sec. IV.

II. MODEL AND METHODS

In the tight-binding representation, the Hamiltonian of the complex honeycomb lattice p–n junction [see Fig. 1(a)] is given by[36]

$$H = \sum_i \epsilon_i a_i^\dagger a_i + \sum_{\langle i,j \rangle} t e^{i\phi_{ij}} a_i^\dagger a_j, \tag{1}$$

where $a_i^\dagger$ and a_i are the creation and annihilation operators at the discrete site i, and ϵ_i is the on-site energy. In the left and right leads, $\epsilon_i = E_L$ or E_R, which can be tuned by the gate voltages.[37] The potential profile from the left to the right leads is assumed to be linear, i.e., $\epsilon_i = k(E_R - E_L)/(2L-2) + E_L + w_i$, where $k = 0, 1, 2, \ldots, 2L+1$, L is the length of the center region, and w_i is the on-site disorder energy. Here, w_i is uniformly distributed in the range of disorder intensity $[-W/2, W/2]$, with W denoting the disorder strength. The center region is described by the width N and length L. A representative system with $N = 2$ and $L = 4$ is illustrated in Fig. 1(a). The second term in the Hamiltonian describes the nearest-neighbor hopping. In the presence of a perpendicular magnetic field B, a phase ϕ_{ij} is added to the hopping term, where $\phi_{ij} = \int_i^j \mathbf{A} \cdot d\mathbf{l}/\phi_0$. Here, the vector potential is $\mathbf{A} = (-B_y, 0, 0)$, and the flux quantum $\phi_0 = \hbar/e$.

The current flowing through the honeycomb lattice p–n junction is calculated using the Landauer–Büttiker formalism,[38,39]

$$J = (2e/h) \int d\epsilon T_{LR}(\epsilon)[f_L(\epsilon) - f_R(\epsilon)], \tag{2}$$

where $f_\alpha(\epsilon) = 1/\{exp[(\epsilon - eV_a)/k_BT] + 1\}(\alpha = L, R)$ is the Fermi distribution function for the left and right graphene leads. Here, the transmission coefficient through the p–n junction reads[40]

$$T_{LR}(\epsilon) = \mathrm{Tr}[\Gamma_L G^r \Gamma_R G^a], \tag{3}$$

where $\Gamma_\alpha(\epsilon) = i[\Sigma_\alpha^r(\epsilon) - \Sigma_\alpha^a(\epsilon)]$ is the line-width function, with $\alpha = L, R$ denoting the left and right leads. The retarded and advanced Green functions satisfy $G^r(\epsilon) = [G^a(\epsilon)]^\dagger = [\epsilon I - H_z - \Sigma_L^r - \Sigma_R^r]^{-1}$, where H_z is the Hamiltonian matrix of the central region and I is the unit matrix. The retarded self-energy Σ_α^r (arising from coupling to lead α) can be calculated numerically.[41–43] After obtaining the current J, the linear conductance is given by $G = \lim_{V\to 0} dJ/dV$.

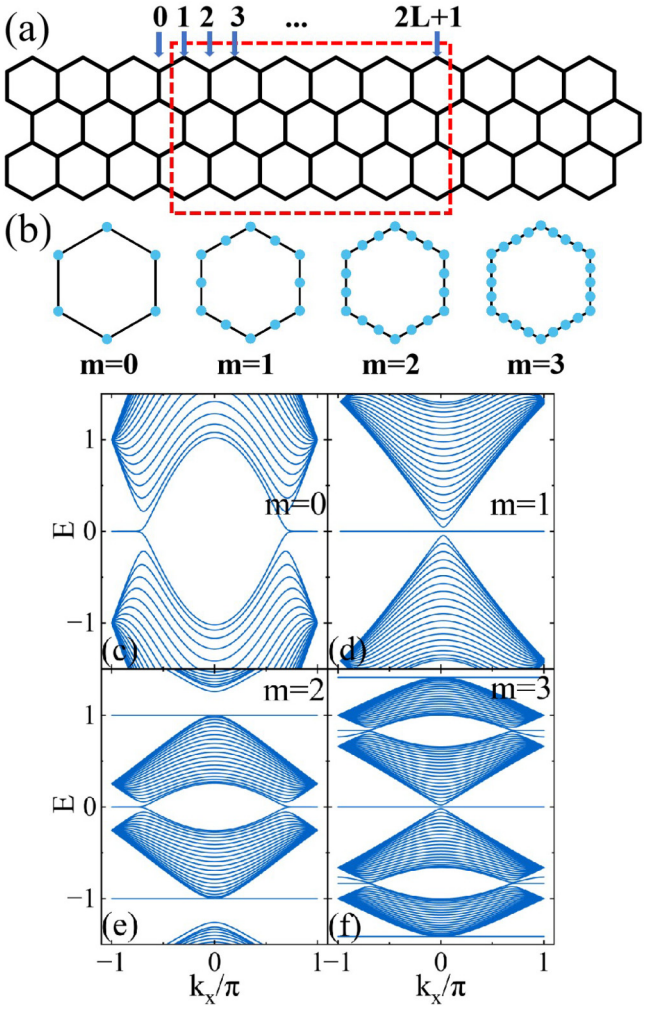

FIG. 1. (a) Schematic of the a zigzag-edged honeycomb lattice p–n junction. (b) Schematic of the CHC lattice, where $m = 0, 1, 2, 3$ from left to right (m is the number of hub atoms on each hexagon edge). The corresponding band structures of CHC lattices with $m = 0, 1, 2, 3$ are shown in (c)–(f), respectively, with system width $N = 10$.

In the following numerical calculations, we adopt the hopping energy $t \approx 2.75$ eV as the energy unit. Since t corresponds to a temperature of 10^4 K, we set the temperature to 0 K in the calculations. The system width N is fixed to 50 for each curve, except in Fig. 3. The nearest-neighbor carbon–carbon distance is denoted as a. The magnetic field is parameterized by ϕ, where $\phi \equiv (3\sqrt{3}/4)a^2B/\phi_0$. Here, $(3\sqrt{3}/2)a^2B$ represents the magnetic flux through the honeycomb lattice. In experiments, the charge

concentration at the p–n junction interface does not change suddenly. Therefore, in our model, the potential in the central region of the p–n junction varies linearly from E_L to E_R.

III. RESULTS AND DISCUSSION

First, we investigate the conductance of the CHC lattice. Figure 2 shows the relationship between the conductance and the right lead energy E_R without a magnetic field, where $E_L = -0.1t$. When $E_L < 0$ and $E_R < 0$, the central region corresponds to a n–n junction, and the conductance G exhibits approximate quantization. Due to the limited number of transverse subbands with finite width, G exhibits a series of equidistant plateaus. The conductance plateau values of $m = 0$ and $m = 2$ lattices are $(2n+1)\cdot 2e^2/h$, while for $m = 1$ and $m = 3$ lattices, the conductance plateau values are $n \cdot 2e^2/h$ $(n = 0, 1, 2, \ldots)$. This arises from their distinct energy band structures.

From the energy band structures of the honeycomb lattices [see Figs. 1(c)–1(f)], the structures of the $m = 0$ (graphene) and $m = 2$ lattices near the Fermi level E_F are similar. They exhibit a unique energy band structure, namely, the straw-hat edge structure, which provides two transmission channels and, thus, increases the number of conducting channels.[44] Especially when $m = 2$, this unique energy band structure exists in the low-energy region. When E_R ranges from -0.1 to $-0.25t$, the number of channels increases, resulting in a significantly higher conductance G than that of other CHC lattices. For $m = 1$ and $m = 3$, a flatband exists at $E = 0$, which distinguishes them from $m = 0$ and $m = 2$, notably, $m = 3$ exhibits two additional flatbands. The number of central atoms (m) correlates with the number of flatbands.[29] Additionally, a bandgap appears near Fermi level E_F, resulting in zero conductance near the right lead energy $E_R = 0$. For $E_R < E_L$, no higher conductance plateaus emerge due to the fixed number of subbands in the left region.

On the other hand, when $E_L < 0$ and $E_R > 0$, the central region corresponds to a p–n junction, where the conductance G is no longer quantized and the plateaus disappear. For $m = 0$ and $m = 2$, the conductance G of the p–n junction (where $E_L < 0$ and $E_R > 0$) is consistently smaller than the corresponding plateau value of the n–n junction (where $E_L < 0$ and $E_R < 0$). The conductance of the p–n junction is due to the Klein tunneling process.[36] With increasing L, the Klein tunneling process weakens, resulting in a slight decrease in conductance. From Fig. 2(c), the conductance of $m = 2$ decreases at $E_R = 0.25t$. This is because the energy band no longer exhibits the straw-hat structure with two transmission channels at $E_R = 0.25t$. For $m = 1$ and $m = 3$, the conductance G in the p–n junction ($E_L < 0, E_R > 0$) exhibits obvious oscillations with increasing E_R, accompanied by a series of peaks, as shown in Figs. 2(b) and 2(d).

Figure 3 shows the relationship between conductance G and right lead energy E_R at different widths, where the length L of the central region is 10 and $E_L = -0.1t$. For the n–n junction (where $E_L < 0$ and $E_R < 0$), the plateau values of conductance for $m = 0, 2$ correspond to $(2n+1)\cdot 2e^2/h$, while those for $m = 1, 3$ correspond to $n \cdot 2e^2/h$ $(n = 0, 1, 2, \ldots)$. When the right lead energy $E_R = 0$, the conductance for $m = 1, 3$ is 0, which is consistent with the conclusion in Fig. 2 above. For the p–n junction (where $E_L < 0$ and $E_R > 0$), we find that the conductance peaks of the CHC lattice for $m = 1, 3$ increase with increasing width of the central region when the length of the central region is fixed. This is because the number of subbands in the left region increases with increasing width of the central region, thereby increasing the conductance. Meanwhile, the peak positions remain unchanged, which differs from the oscillatory behavior observed in Fig. 2.[45,46]

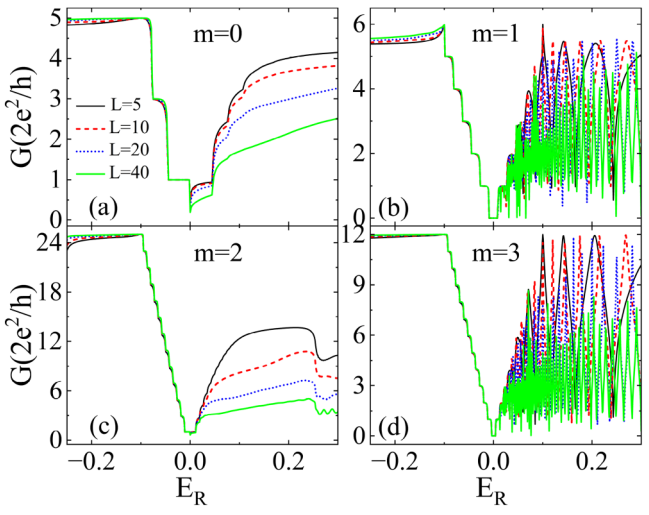

FIG. 2. Relationship between conductance G and right lead energy E_R for different central region lengths L. (a) corresponds to $m = 0$, (b) $m = 1$, (c) $m = 2$, and (d) $m = 3$, with other parameters fixed as left lead energy $E_L = -0.1t$, system width $N = 50$ and magnetic flux $\phi = 0$.

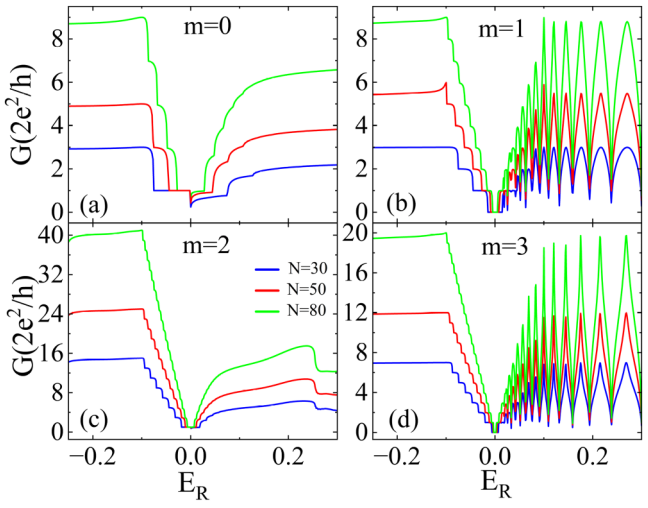

FIG. 3. Relationship between conductance G and right lead energy E_R for different central region widths N. (a) corresponds to $m = 0$, (b) $m = 1$, (c) $m = 2$, and (d) $m = 3$. The blue line corresponds to $N = 30$, the red line to $N = 50$, and the green line to $N = 80$. Other parameters are fixed to left lead energy $E_L = -0.1t$, central region length $L = 10$ and magnetic flux $\phi = 0$.

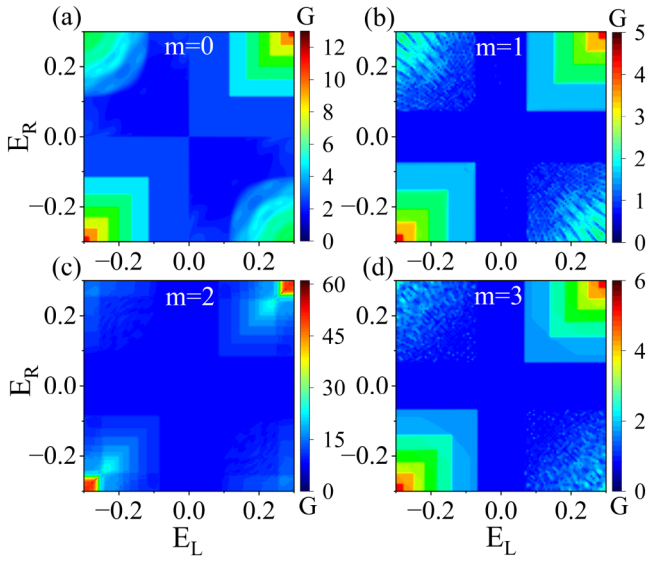

FIG. 4. Relationship between conductance G (in units of $2e^2/h$) and left/right lead energies E_L and E_R, with central region length $L = 10$ and magnetic flux $\phi = 0.003$. (a) corresponds to $m = 0$, (b) $m = 1$, (c) $m = 2$, and (d) $m = 3$.

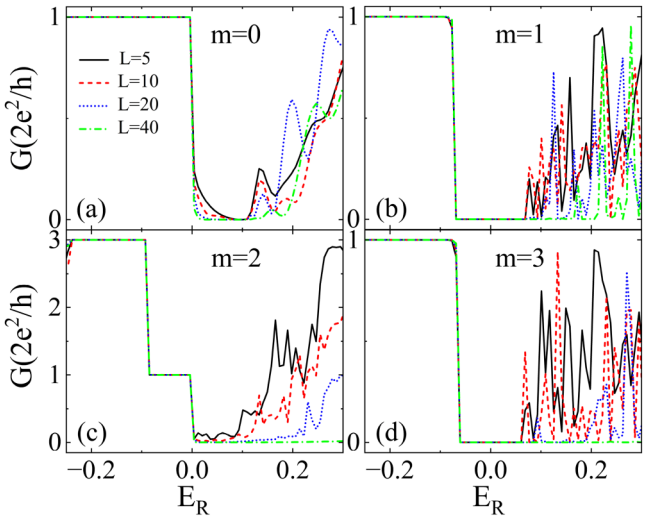

FIG. 5. Relationship between conductance G and right lead energy E_R for different central region lengths L. (a) corresponds to $m = 0$, (b) $m = 1$, (c) $m = 2$, and (d) $m = 3$, with other parameters fixed as left lead energy $E_L = -0.1t$, system width $N = 50$ and magnetic flux $\phi = 0.003$.

When a vertical magnetic field is introduced, electrons move clockwise or counterclockwise along the edge of the nanoribbon. The conductance of the honeycomb lattice varies with the left and right lead energies E_L and E_R, as shown in Fig. 4. Under a strong magnetic field, Landau energy levels are formed. In the n–n junction ($E_L < 0, E_R < 0$), the conductance evolves into a Hall plateau with a plateau value of $\min(|\nu_L|, |\nu_R|)e^2/h$ (in $2e^2/h$), where ν_α is the filling factor of lead α ($\alpha = L$ or R).[15,36] At fixed filling factors ν_L and ν_R, the conductance G is approximately constant. For example, in the n–n junction of the CHC lattice with $m = 1$, when $E_L = -0.1$ ($\nu_L = -2$) and $E_R = -0.2$ ($\nu_L = -6$), the conductance value is $2e^2/h$. However, there is no conductance plateau in the p–n junction ($E_L < 0, E_R > 0$). For $m = 1$ and $m = 3$, the conductances oscillate periodically as E_L and E_R vary [see Figs. 4(b) and 4(d)]. This is because under a uniform magnetic field, the Hall edge states of electrons and holes are formed in the n-region and the p-region, and the transport direction of electrons is opposite to that of holes. At the interface of electron and hole Hall edge states, the formation of electron–hole Hall edge mixed states leads to partial conductance.

Then, we investigate the effects of the central region length and the magnetic field, the relationship between the conductance G and the right lead energy E_R under a magnetic flux $\phi = 0.003$ is calculated, as shown in Figs. 5(a)–5(d). For $m = 0$ and $m = 2$, the conductance plateaus evolve into Hall plateaus in the n–n junction ($E_L < 0, E_R < 0$). In the p–n junction ($E_L < 0, E_R > 0$), there is no conductance plateau, and the conductance is contributed by electron–hole Hall edge mixed states. For $L = 20$, when the filling factor is small (i.e., $0 < E_R < 0.1t$), carriers tend to be localized into states, and mixed states are difficult to form, resulting in nearly zero conductance. When the filling factor is larger ($E_R > 0.1t$), mixed states are formed, and the conductance appears. When the central region length $L = 40$, the Hall edge states of electrons and holes are spatially separated, resulting in strong suppression of the conductance G. For $m = 1$ and $m = 3$ [see Figs. 5(b) and 5(d)], Hall plateaus are formed in the n–n junction ($E_L < 0, E_R < 0$). In the p–n junction ($E_L < 0, E_R > 0$), the system conductance oscillates. Due to the bandgap near the Fermi level, the conductance in the middle region is zero. The oscillation strength of the conductance depends on the central region length of the p–n junction. With increasing L, the oscillation intensity diminishes and conductance G decreases. For when L is small, the Hall edge states of electrons and holes can spatially form mixed states. When L is large, the Hall edge states of electrons and holes are spatially separated and, thus, cannot form mixed states, leading to a decrease in conductance G.

Next, we focus on the case of $m = 1$. We investigate the influence of disorder on the conductance of the CHC lattice in more detail. Figure 6 shows the relationship between conductance G and right lead energy E_R under zero magnetic field of different disorder strengths W with the $m = 1$ CHC lattice. For the p–n junction system of the $m = 1$ CHC lattice under zero magnetic field, in the n–n junction, when the disorder strength $W = 0.05$, the conductance still retains the original plateau, which matches that at $W = 0$. With increasing disorder strength W, the conductance G gradually decreases, the number of plateau steps reduces, and the plateau shifts closer to the Fermi level. In the p–n junction, the oscillatory behavior is suppressed by the addition of disorder, the oscillations disappear, and new plateaus form. For example, at a disorder strength of $W = 0.05$, the conductance G forms a new

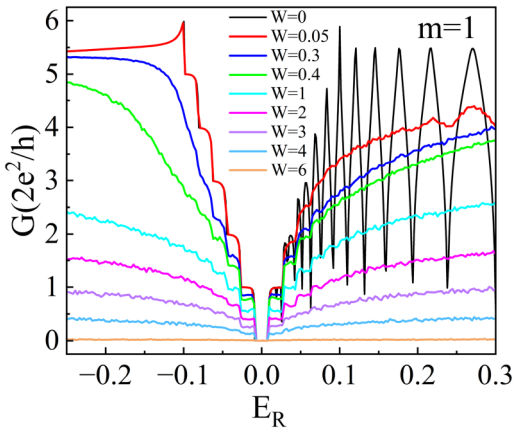

FIG. 6. The relationship between conductance G and right lead energy E_R for the $m = 1$ CHC lattice under different disorder strengths W and zero magnetic field, with other parameters fixed as $E_L = -0.1t$, $L = 10$, and $N = 50$.

plateau, with the plateau value is 1 (in units of $2e^2/h$). With increasing disorder strength W, the overall conductance decreases, but the number of plateaus increases. However, when W reaches 6, the conductance G becomes very small (nearly zero), and no conductance plateaus are observed. This arises because electrons transition from macroscopically mobile extended states to completely localized bound states. In the low-energy region near the Fermi level, plateaus are observed on both sides of $E_R = 0$, and these plateaus are symmetric about $E_R = 0$, forming a bidirectional conduction channel. This provides a new approach for investigating the quantum transport properties of topological materials.

Finally, we investigate the influence of disorder intensity on the conductance of the CHC lattice under a magnetic field. In Fig. 7, the relationship between conductance G and right lead energy E_R is depicted at fixed $E_L = -0.1t$ and magnetic flux $\phi = 0.003$. Previous studies[36] have found that disorder enhances the conductance of graphene ($m = 0$) p–n systems under a magnetic field. Over a certain range of disorder intensity, the ideal plateau value can be achieved. As the disorder intensity further increases, the conductance begins to decrease. For very large disorder intensity W, the system transitions to an insulating state.

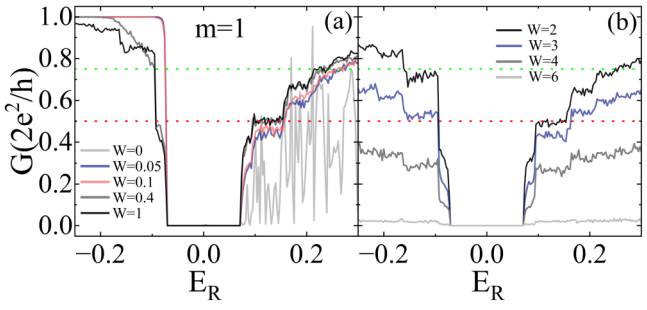

FIG. 7. Relationship between conductance G and right lead energy E_R under different disorder strengths W. (a) and (b) correspond to $m = 1$, with other parameters fixed as $E_L = -0.1t$, $L = 10$, $N = 50$, and magnetic flux $\phi = 0.003$.

For the CHC lattice with $m = 1$, when $W = 0$, a Hall plateau appears in the conductance G for the n–n junction, while the p–n junction exhibits oscillatory behavior with peak values. With increasing disorder strength W from 0, the Hall plateau in the n–n junction is unaffected by weak disorder, and the plateau value ($\min(|v_L|, |v_R|)e^2/h$) is maintained. In the p–n junction, the conductance peak values gradually flatten out, and the oscillatory behavior disappears. This is because the oscillation under high magnetic field is suppressed in disorder state. In particular, for disorder strength W in the range of 0.05–4, a conductance plateau emerges. According to the ideal conductance plateau value ($[|v_L||v_R|/(|v_L| + |v_R|)]e^2/h$), when $E_L = -0.1$ ($v_L = -2$) and $E_R = 0.1$ ($v_R = 2$), the ideal conductance plateau value is, thus, e^2/h, as shown by the red dashed line in Fig. 7. For disorder strength W in the range of 0.4–2, the actual plateau value agrees with the ideal conductance plateau value e^2/h. However, for other disorder strengths, the actual plateau value is lower than the ideal one e^2/h. For a higher filling factor, under $E_L = -0.1$ ($v_L = -2$) and $E_R = 0.2$ ($v_R = 6$), the ideal conductance plateau value is $(3/2)e^2/h$, as shown by the green dashed line in Fig. 7. The conductance also increases due to the enhancement effect of disorder, and a new plateau emerges; however, its values are consistently lower than the ideal plateau values. For example, when $E_L = -0.1$ ($v_L = -2$) and $E_R = 0.2$ ($v_R = 6$), the conductance plateau value at disorder strength $W = 3$ is $(11/10)e^2/h$, which is lower than the ideal conductance plateau value $(3/2)e^2/h$. For very large disorder strength (e.g., $W = 6$ or above), the system transitions to an insulating state. For higher filling factors, the conductance G becomes very small, (approaching zero), and the conductance plateau no longer appears. This is because complete mixing of all states is difficult at high filling factors, and the system enters an insulating state before a fully mixed state can form. These findings are in good agreement with previous studies. In particular, disorder does not affect the bandgap width.

IV. CONCLUSIONS

In summary, we investigate the transport properties of the CHC lattice p–n junction using the non-equilibrium Green's function method and the tight-binding approximation Hamiltonian. In the absence of an external magnetic field, the conductance of the CHC lattice exhibits a series of equidistant plateaus in the n–n junction. In the p–n junction, CHC lattices with $m = 1$ and $m = 3$ exhibit oscillatory behavior. Upon application of an external magnetic field, the conductance plateau in the n–n junction evolves into a Hall platform. The conductance of the p–n junction still oscillates. For CHC lattices with $m = 1$ and $m = 3$, the zero conductance in the middle region arises from the forbidden band. For the CHC lattice p–n junction system with $m = 1$ without magnetic field, a bidirectional conduction channel forms near right lead energy $E_R = 0$ under the influence of disorder. For CHC lattice p–n junction systems with $m = 1$ under a magnetic field, the introduction of disorder can enhance conductance, but the ideal plateau

is only maintained within a specific range of disorder strength. If the disorder strength exceeds a critical limit, the system transitions to an insulating state.

ACKNOWLEDGMENTS

This work was supported by the National Natural Science Foundation of China (NSFC) (Grant No. 11874139) and the Natural Science Foundation of Hebei province (Grant No. A2019205190).

AUTHOR DECLARATIONS

Conflict of Interest

The authors have no conflicts to disclose.

Author Contributions

Yao Zhang: Formal analysis (equal); Writing – original draft (equal). **Xing Wang:** Formal analysis (equal); Methodology (equal). **Yu-Xian Li:** Formal analysis (equal); Funding acquisition (supporting); Investigation (equal); Methodology (supporting); Supervision (equal); Writing – review & editing (equal).

DATA AVAILABILITY

The data that support the findings of this study are available from the corresponding author upon reasonable request.

REFERENCES

[1]K. S. Novoselov, A. K. Geim, S. V. Morozov *et al.*, "Two-dimensional gas of massless Dirac fermions in graphene," Nature **438**, 197–200 (2005).
[2]V. P. Gusynin and S. G. Sharapov, "Unconventional integer quantum Hall effect in graphene," Phys. Rev. Lett. **95**, 146801 (2005).
[3]J. H. Bardarson, J. Tworzydło, P. W. Brouwer *et al.*, "One-parameter scaling at the Dirac point in graphene," Phys. Rev. Lett. **99**, 106801 (2007).
[4]K. Nomura, M. Koshino, and S. Ryu, "Topological delocalization of two-dimensional massless Dirac fermions," Phys. Rev. Lett. **99**, 146806 (2007).
[5]C. H. Park, Y. W. Son, L. Yang *et al.*, "Electron beam supercollimation in graphene superlattices," Nano Lett. **8**, 2920–2924 (2008).
[6]L. Oroszlány, P. Rakyta, A. Kormányos *et al.*, "Theory of snake states in graphene," Phys. Rev. B **77**, 081403 (2008).
[7]Y. Kim, A. C. Balram, T. Taniguchi *et al.*, "Even denominator fractional quantum Hall states in higher Landau levels of graphene," Nat. Phys. **15**, 154–158 (2019).
[8]C. Mullan, S. Slizovskiy, J. Yin *et al.*, "Mixing of Moiré-surface and bulk states in graphite," Nature **620**, 756–761 (2023).
[9]J. P. Esparza and V. Juričić, "Exceptional magic angles in non-Hermitian twisted bilayer graphene," Phys. Rev. Lett. **134**, 226602 (2025).
[10]A. H. Castro Neto, F. Guinea, N. M. R. Peres *et al.*, "The electronic properties of graphene," Rev. Mod. Phys. **81**, 109 (2009).
[11]M. Saeidi and M. Esmaeilzadeh, "Valley-dependent transmission properties of tilted massless Dirac fermions in a two-dimensional salt $n-p-n$ junction," Phys. Rev. B **110**, 235304 (2024).
[12]K. S. Novoselov, A. K. Geim, S. V. Morozov *et al.*, "Electric field effect in atomically thin carbon films," Science **306**, 666–669 (2004).
[13]Y. B. Zhang, Y. W. Tan, H. L. Stormer *et al.*, "Experimental observation of the quantum Hall effect and Berry's phase in graphene," Nature **438**, 201–204 (2005).
[14]N. Mazzucca, B. M. Kousa, and K. Watanabe, "Half-integer quantum Hall states in two-dimensional graphite," Phys. Rev. Lett. **134**, 176302 (2025).
[15]J. R. Williams, L. DiCarlo, and C. M. Marcus, "Quantum Hall effect in a gate-controlled $p-n$ junction of graphene," Science **317**, 638–641 (2007).
[16]N. Mazzucca, B. M. Kousa, K. Watanabe *et al.*, "Half-integer quantum Hall states in two-dimensional graphite," Phys. Rev. Lett. **134**, 176302 (2025).
[17]D. Abanin and L. S. Levitov, "Quantized transport in graphene $p-n$ junctions in a magnetic field," Science **317**, 641–643 (2007).
[18]K. S. Novoselov, E. Mccann, S. V. Morozov *et al.*, "Unconventional quantum Hall effect and Berry's phase of 2π in bilayer graphene," Nat. Phys. **2**, 177–180 (2006).
[19]B. Zhou and Y. H. Zhang, "New classes of quantum anomalous Hall crystals in multilayer graphene," Phys. Rev. Lett. **135**, 036501 (2025).
[20]M. I. Katsnelson, K. S. Novoselov, and A. K. Geim, "Chiral tunnelling and the Klein paradox in graphene," Nat. Phys. **2**, 620–625 (2006).
[21]B. Sutherland, "Localization of electronic wave functions due to local topology," Phys. Rev. B **34**, 5208 (1986).
[22]B. Dóra, J. Kailasvuori, and R. Moessner, "Lattice generalization of the Dirac equation to general spin and the role of the flat band," Phys. Rev. B **84**, 195422 (2011).
[23]J. D. Malcolm and E. J. Nicol, "Magneto-optics of general pseudospin-s two-dimensional Dirac-Weyl fermions," Phys. Rev. B **90**, 035405 (2014).
[24]J. Vidal, P. Butaud, B. Douçot *et al.*, "Disorder and interactions in Aharonov-Bohm cages," Phys. Rev. B **64**, 155306 (2001).
[25]J. M. Lee, C. Geng, J. W. Park *et al.*, "Stable flatbands, topology, and superconductivity of magic honeycomb networks," Phys. Rev. Lett. **124**, 137002 (2020).
[26]J. W. Park, G. Y. Cho, J. Lee *et al.*, "Emergent honeycomb network of topological excitations in correlated charge density wave," Nat. Commun. **10**, 4038 (2019).
[27]D. Cho, Y. H. Cho, S. W. Cheong *et al.*, "Interplay of electron-electron and electron-phonon interactions in the low-temperature phase of $1T-TaS_2$," Phys. Rev. B **92**, 085132 (2015).
[28]Z. Qi, E. Bobrow, and Y. Li, "Robust flat bands with tunable energies in honeycomb superlattices," arXiv:2012.07806 (2020).
[29]J. Wang and J. F. Liu, "Super-Klein tunneling and electron-beam collimation in the honeycomb superlattice," Phys. Rev. B **105**, 035402 (2022).
[30]K. Y. Lyu, X. Wang, and Y. X. Li, "Enhanced Seebeck and Nernst effects in the complex honeycomb lattice," Phys. Rev. B **111**, 235404 (2025).
[31]E. Illes and E. J. Nicol, "Klein tunneling in the $\alpha-T_3$ model," Phys. Rev. B **95**, 235432 (2017).
[32]Y. Betancur-Ocampo, G. Cordourier-Maruri, V. Gupta *et al.*, "Super-Klein tunneling of massive pseudospin-one particles," Phys. Rev. B **96**, 024304 (2017).
[33]S. G. Cheng, Y. X. Xing, J. Wang *et al.*, "Controllable Andreev retroreflection and specular Andreev reflection in a four-terminal graphene-superconductor hybrid system," Phys. Rev. Lett. **103**, 167003 (2009).
[34]C. H. Lewenkopf and E. R. Mucciolo, "The recursive Green's function method for graphene," J. Comput. Electron. **12**, 203–231 (2013).
[35]Z. H. Qiao, J. Jung, Q. Niu *et al.*, "Electronic highways in bilayer graphene," Nano Lett. **11**, 3453–3459 (2011).
[36]W. Long, Q. F. Sun, and J. Wang, "Disorder-induced enhancement of transport through graphene $p-n$ junctions," Phys. Rev. Lett. **101**, 166806 (2008).
[37]K. Shizuya, "Persistent current distributions along a $p-n$ junction in graphene in a magnetic field," Phys. Rev. B **110**, 155437 (2024).
[38]J. T. Song, H. W. Liu, J. Liu *et al.*, "Quantum interference in topological insulator Josephson junctions," Phys. Rev. B **93**, 195302 (2016).
[39]J. Liu, H. W. Liu, J. T. Song *et al.*, "Superconductor-graphene-superconductor Josephson junction in the quantum Hall regime," Phys. Rev. B **96**, 045401 (2017).
[40]Y. F. Zhou, H. Jiang, X. C. Xie *et al.*, "Two-dimensional lattice model for the surface states of topological insulators," Phys. Rev. B **95**, 245137 (2017).
[41]M. P. Lopez Sancho, J. M. Lopez Sancho, J. Rubio *et al.*, "Quick iterative scheme for the calculation of transfer matrices: Application to Mo (100)," J. Phys. F **14**, 1205 (1984).
[42]D. H. Lee and J. D. Joannopoulos, "Simple scheme for surface-band calculations. II. The Green's function," Phys. Rev. B **23**, 4997 (1981).

[43]M. P. Lopez Sancho, J. M. Lopez Sancho, J. Rubio *et al.*, "Highly convergent schemes for the calculation of bulk and surface Green functions," J. Phys. F **15**, 851 (1985).
[44]C. Fang, Y. Chen, H. Y. Kee *et al.*, "Topological nodal line semimetals with and without spin-orbital coupling," Phys. Rev. B **92**, 081201(R) (2015).
[45]S. G. Cheng, "Magnetic field mediated conductance oscillation in graphene $p-n$ junctions," J. Phys.: Condens. Matter **30**, 165301 (2018).
[46]P. P. Zhang, C. Wang, Y. X. Li *et al.*, "The transport properties of Kekulé-ordered graphene $p-n$ junction," New J. Phys. **25**, 113021 (2023).